

Quaternary Heusler Alloy: An Ideal Platform to Realize Triple Point Fermion

C. K. Barman,^{1,*} Chiranjit Mondal,^{2,*} Biswarup Pathak,² and Aftab Alam^{1,†}

¹*Department of Physics, Indian Institute of Technology, Bombay, Powai, Mumbai 400 076, India*

²*Discipline of Metallurgy Engineering and Materials Science, IIT Indore, Simrol, Indore 453552, India*

(Dated: September 20, 2018)

The existence of three fold rotational, mirror and time reversal symmetries often give rise to the triply degenerate nodal point (TP) in the band structure of a material. Based on point group symmetry analysis and first principle electronic structure, we predict, in this article, a series of quaternary Heusler alloys host an ideal platform for the occurrence of TP. We simulated, the projection of these TPs onto the (111) and (100) surfaces lead to form topological Fermi arcs, which may further be detected by scanning tunneling spectroscopy and angle resolved photoemission spectroscopy. These Fermi arcs arise due to the symmetry protected band degeneracies, which are robust and can not be avoided due to the non-trivial band topology. Interestingly the TPs, in these class of Heusler alloys are far away from the Γ point along C_3 axes, which allow to overcome the experimental difficulties over previously studied hexagonal and HgTe-type compounds.

Introduction: Nontrivial Fermi surface topology in metals and semimetals has recently been more exciting research frontiers over gaped systems. Unlike topological insulators, topological metals and semimetals¹⁻⁴ are interesting not only because of their rich surface physics but also for the exotic nature of linear band crossing nature in bulk. The semimetals have further been classified into Dirac semimetal (DSM),⁵⁻¹² Weyl Semimetal (WSM),¹³⁻²⁰ and Nodal-line semimetal (NLS)²¹⁻²⁸ depending on the dimensionality of the band crossing points and Fermi surface topology in the momentum space. The Fermi surface of DSM and WSM have been experimentally verified to be zero-dimensional discrete points in the bulk Brillouin zone (BZ), where as, it is one-dimensional close loop for NLS. The quasi-particle counter part to elementary Dirac and Weyl fermion in the standard model have been mimicked near the four fold Dirac nodes and two fold Weyl nodes in their low energy excitations. In contrast, NLS does not have a direct analogue to the elementary quasi particle in the high energy physics.

Another example of quasi-particle excitation in condensed matter physics which does not have elementary particle counter part in the quantum field theory is topological triple point semimetal (TPSM).²⁹⁻³⁶ TPSM is essentially protected by crystal point group symmetry and believed to be same kind of an intermediate state between four fold Dirac fermion and two fold Weyl fermion system. For example, having three fold rotational symmetry with a vertical mirror plane in a non-magnetic crystal can lead to a pair of triply degenerate nodal points along C_3 axis in the absence of crystal inversion. A Dirac node can be achieved by keeping the inversion intact in such an symmetry environment. If vertical mirror symmetry is further broken, it produces four Weyl nodes from two triple points reducing the band degeneracies.

Although it is theoretically quite straightforward to achieve TPSM states but realizing such states near the Fermi level is quite fragile. Moreover, stabilizing the nodes are too hard as they need fine tuning of chem-

ical composition. Three component fermion which is prohibited in the presence of Lorentz invariance have been predicted in both symmorphic and non-symmorphic space group symmetry.²⁹ However, the hunt for a suitable material class is still ongoing for table top experiment; such as, observation of Fermi arcs using surface sensitive photo emission spectroscopy. Some of the materials such as WC,²⁹ ZrTe,³⁷ MoP,³⁸ MgTa_{2-x}Nb_xN₃,^{39,40} strained-HgTe⁴¹ which have been predicted to be three component Fermion system belongs to hexagonal space group. For such a space group material, (001) surface is the most natural choice to cleave. As the TPs are protected by C_{3v} point group symmetry, they lie on the C_3 axis. Therefore, projecting the TPs on (001) facet of hexagonal compound results in disappearance of the TP induced Fermi arcs. This scenario has been observed in case of MoP.³⁸ Very recently, a bunch of ternary half-Heusler compounds^{42,43} have been theoretically predicted to host TPSM state along Γ - L direction in BZ. As the little group of Γ for these compounds is T_d , they contain four independent C_3 axis. Projecting the TPs on (111) surface will produce six Fermi arcs that connect the projected triple point nodes as described in Ref.^[42,43]. This class of material readily solve the previously described problem on hexagonal systems. Unfortunately, the position of TPs on the C_3 axis in some of these compounds⁴¹⁻⁴³ are extremely close to Γ point. This results in extremely small Fermi arcs on its (111) facets, identification of which is a major constraint in experimental measurements.

Here, we introduce another class of Heusler alloy which is quaternary and produce a triple point node along the Γ - L direction in BZ. In this class of quaternary Heusler alloy, the three fold degenerate nodal point occur far away from Γ point which consequently yields a decent sized Fermi arcs. This, in turn immediately removes the experimental constraints over some of the previous studies in HgTe⁴¹ and ternary Heusler alloys.^{42,43}

Computational Details: First principle calculations were performed using Vienna Ab-initio Simulation Pack-

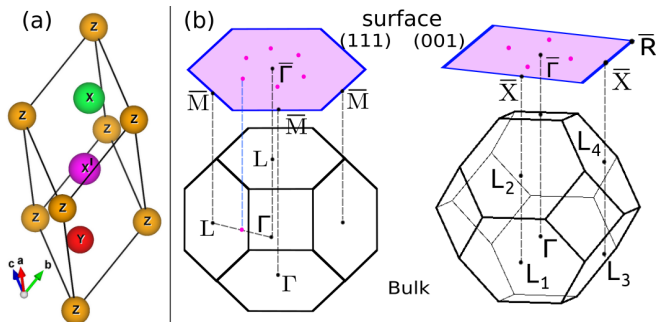


FIG. 1. (Color online) (a) Primitive crystal structure of quaternary Heusler alloy $XX'YZ$, (b) pictorial depiction of bulk and surface BZ with high symmetry points. The projection of L points on both (111) and (001) surfaces are shown by dotted lines. Magenta dots are projection of TPs on surface.

age (VASP)^{44,45} based on density functional theory (DFT). To describe the exchange and correlation functional, we adopt generalized gradient approximation by Perdew-Burke-Ernzerhof (PBE).⁴⁵ Plane wave basis set using Projector Augmented Wave (PAW)⁴⁶ method was used with an energy cut off 500 eV. Total energy (force) was converged upto 10^{-6} eV/cell (0.001 eV/Å). Brillouin zone(BZ) integrations were performed using $12 \times 12 \times 12$ Γ -centered k-mesh. The spin-orbital coupling (SOC) effect was included in all the calculations. A tight binding model was constructed using maximally localized wannier functions (MLWF)⁴⁷⁻⁴⁹ to closely reproduce the bulk band structure. The iterative Greens function⁵⁰⁻⁵² method implemented in Wannier_tool package⁵³ was employed to calculate the Fermi arcs and surface dispersions.

Results and Discussion: Here, in this study, we present a bunch of quaternary half-Heusler alloy, which provide an ideal platform (as the TPs are located far away from zone center and it readily removes the bottleneck of cleaved surface in hexagonal system) to realize triple point semimetal states from both experimental and theoretical front. The crystal structure and Brillouin zone (BZ) of quaternary Heusler alloy (space group $F\bar{4}3m$ ⁵⁴) is described in Fig. 1. The primitive cell possesses four atoms X, X', Y and Z at wyckoff positions 4c, 4d, 4b and 4a respectively. Figure 1(b,c) shows the BZ of bulk cell and the projected BZ for (111) and (001) surface. The magenta dots on surface BZ will be discussed later.

We take LiMgPdSb as a prototype system and provide a detailed calculation on it. The electronic structure of LiMgPdSb compound without SOC is shown in Fig. 2(a). The crystal structure of cubic Heusler alloy⁵⁴ with space group 216 possesses the T_d point group symmetry. To get better insight about the non-triviality and the formation of TP, we describe band symmetries based on point group analysis. In Fig. 2(a), due to the cubic tetrahedral crystal field splitting, the valence band maxima (VBM)

at Γ point hold three fold degenerate A_5 representation which is composed of (p, d) -orbitals. While the second highest occupied s-like band posses A_1 representation of T_d point group. Along Γ -L direction, the bands have B_1 & B_3 representation under C_{3v} point group, which contain four independent C_3 axis along Γ -L direction with three vertical mirror plane (σ_v) of symmetry.

In the presence of SOC, the three fold degenerate A_5 states at Γ point split into four fold Γ_8 ($J_z = \pm \frac{3}{2}$) states and two fold degenerate Γ_7 ($J_z = \pm \frac{1}{2}$) states. Similarly, the A_1 state transform into Γ_6 ($J_z = \pm \frac{1}{2}$). Γ_6 , Γ_7 and Γ_8 are the representation of T_d considering the 2π rotation of spin subspace. Now, the s-like Γ_6 state stays, in energy, below the p-like Γ_8 states, resulting an inverted band order between Γ_6 and Γ_8 states. Such non-trivial band topology serves as to conduct unique features on surface dispersion, which will be discussed in details later in the manuscript.

Figure 2(c) describes the the origin of triple point from the perspective of chemical hybridization and crystal field splitting of atomic levels. The Pd atom is located at the tetrahedral position in crystal structure. Without SOC, in the vicinity of Γ point (in region I), $t_{2g}(d_{xy}, d_{yz}, d_{zx})$ orbitals hybridized with Sb(p)-orbitals and form A_5 level near E_F . The $e_g(d_{x^2-y^2}, d_{z^2})$ -orbitals (not shown here) stays far below E_F . On the other-hand, the high energy lying three fold degenerate A_5 states are contributed by Pd(p)-orbitals. In addition, the A_1 state below to that A_5 level are composed of s-like orbitals of (Pd, Mg, Sb) atoms. In region-II at/near Γ -point, the influence of SOC splits the hybridized A_5 state into $J = \frac{1}{2}$ and $J = \frac{3}{2}$ states. Along Γ -L direction, the Γ_8^{pd} splits into Λ_4 , Λ_5 , and Λ_6 states at E_F in the vicinity of triple point as shown in region III, Fig. 2(c). Γ_7^{pd} , on the other hand, goes below to E_F , represented as two-dimensional irreducible representation (IR) Λ_4 .

Now we will discuss the general formation mechanism of triply degenerate nodal points in band structure with the help of point group symmetry analysis. A system having little group of C_{3v} along some high symmetry direction, whose elements are three fold rotation (C_3) and three σ_v mirror, provides two one-dimensional IRs (Λ_5 & Λ_6) and one two-dimensional IR (Λ_4) in its double group representation. In general, the effective mass of Λ_5/Λ_6 and Λ_4 are opposite.⁴² So, there could be some accidental degeneracy between Λ_5/Λ_6 and Λ_4 when they disperse over the BZ along C_{3v} axis. Consider a system which does not have inversion center but preserve the time reversal symmetry, the Kramer's degeneracy will be broken for Λ_4 and Λ_5 over the BZ except at time reversal invariant momenta (TRIM) points. In such a situation the dimension of degeneracy between Λ_5 (or Λ_6) and Λ_4 are three fold at their crossing points. Hence they form triply degenerate nodal points when they cross each other. A cartoon diagram of formation of TP explaining above mechanism, is shown in the Fig. 2(d). The existence of such TP near the Fermi level strongly influence

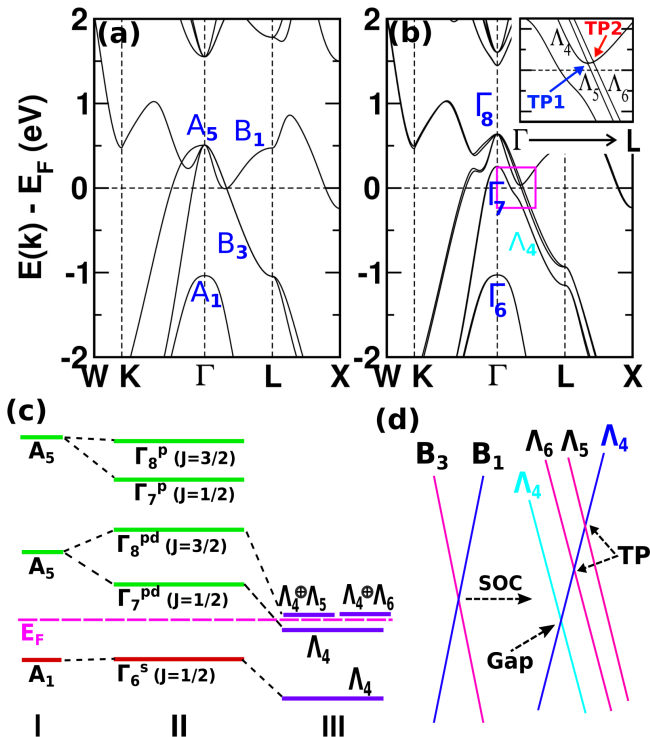


FIG. 2. (Color online) Bulk band structure of LiMgPdSb (a) w/o-soc and (b) w/-soc. The inset in (b) shows the enlarged picture around the triple point crossing region marked by colored box. (c) The schematic representation of band evolution near the Fermi level. Region I represents the combined effect of crystal field splitting and orbital hybridization in the vicinity of Γ point. Region II represents the effect of SOC on band splitting (described in text). Region III is in the vicinity of TP where Γ_8^{pd} bands transformed into degenerate $\Lambda_{4,5,6}$ at E_F and Γ_7^{pd} appear below E_F with Λ_4 character. (d) Schematic illustration for generation of triply degenerate nodal point for non-centro-symmetric crystal with C_{3v} point group. Λ_i (B_i) are the irreducible representations of C_{3v} with(out) SOC effect. The triple points are denoted by TP. Inclusion of SOC generates TPs at the crossing of $\Lambda_{5,6}$ and Λ_4 . The band crossing between two same IRs (Λ_4) opens up a gap as shown by intersection point of indigo and blue color line.

the low energy excitation which in turn provide abnormal transport anomaly, non-trivial Fermi arc topology etc. Interestingly, the above prescription is valid for both symmorphic and non-symmorphic space group.³⁶

Let us now try to understand the realization of triple points in our system LiMgPdSb based on the general mechanism described above. If we closely look at the evolution of bands from w/o-SOC to w/-SOC (i.e. Fig. 2(a) and 2(b)), the transformation of bands (along C_{3v} axes) from simple group to double group follows – $B_1 \rightarrow \Lambda_4$ and $B_3 \rightarrow \Lambda_4 \oplus \Lambda_5 \oplus \Lambda_6$. i.e., B_1 bands transform to Λ_4 bands, where as B_3 bands split into two singly degenerate Λ_5 & Λ_6 bands and one doubly degenerate Λ_4 bands. Fig. 2(b) shows that near Fermi energy Λ_4 , Λ_5 and Λ_6 band almost linear with same slope upto a large mo-

TABLE I. The compounds name, their optimized lattice parameter, number of TPs with their position in terms of energy position ($\Delta\epsilon$) with respect to E_F and distance (Δ_k) in % (along Γ -L line) from Γ point along C_3 axes. The energy position of TP1 for each material is given, while the energy position of TP2 is very close to that of TP1.

Compound	a_{opt} (\AA)	#	Δ_k	$\Delta\epsilon$ (eV)
LiMgPdSb	6.55	TP1	34.07%	0.03
		TP2	36.69%	
LiMgPtSb	6.53	TP1	47.70%	-0.36
		TP2	56.49%	
LiMgAuSn	6.69	TP1	42.36%	0.13
		TP2	46.29%	
LiMgPdSn	6.51	TP1	23.84%	1.72
		TP2	25.62%	
LiMgPtSn	6.49	TP1	37.68%	1.54
		TP2	42.25%	

menta about $0.34k$ along Γ -L direction. Beyond that, the Λ_5 and Λ_6 still disperse linearly towards low energy but Λ_4 changes its mass and disperse almost quadratically towards higher energy and intersect both Λ_5 & Λ_6 . The reason behind these kind of sudden change of slope by Λ_4 band could be due to the band repulsion of another Λ_4 band which originates from the p-like Γ_7 ($J=1/2$) band at Γ point. The intersection points of Λ_4 with Λ_5 and Λ_6 are the triply degenerate nodal points TP1 and TP2 with the position in momentum space to be $(0.170, 0.170, \pm 0.170)\frac{\pi}{c}$ and $(0.183, 0.183, \pm 0.183)\frac{\pi}{c}$ respectively.

Now, given four C_3 axes (Γ -L line) in the bulk BZ, eight pair of TPs form in the first BZ. Projection of three pair of these TPs onto the (111) surface form hexagon surrounding the $\bar{\Gamma}$ point in surface BZ, while the fourth pair of TP exactly projects on the $\bar{\Gamma}$ point. The projection of these six TPs around the $\bar{\Gamma}$ point are pictorially depicted by magenta dots on (111) surface in Fig. 1(b). The TP2 (TP1) in LiMgPdSb compound is around $\sim 36.69\%$ (34.07%) of Γ -L distance away from Γ point which is large enough for experimental observations. The position of these TPs along energy axis also extremely important to be probed from a suitable experiment (photoemission spectroscopy vs. scanning tunneling microscopy). In the present system, TP1 lies extremely close to the Fermi level (E_F); ~ 0.03 eV above E_F . TP2 position is close to TP1.

A similar observation of TPs are also reported on strained HgTe and ternary half-Heusler compounds.⁴¹⁻⁴³ But unfortunately TPs in these materials are close to the Γ point. There exists few other compounds⁴² where the position of TPs lie at large momenta due to the "peculiar double-valley" type dispersion of Λ_4 bands. The mechanism for the formation of triple point nodes in these compounds are quite different compared to our materials. In our case, the emergence of large momenta TPs are in its

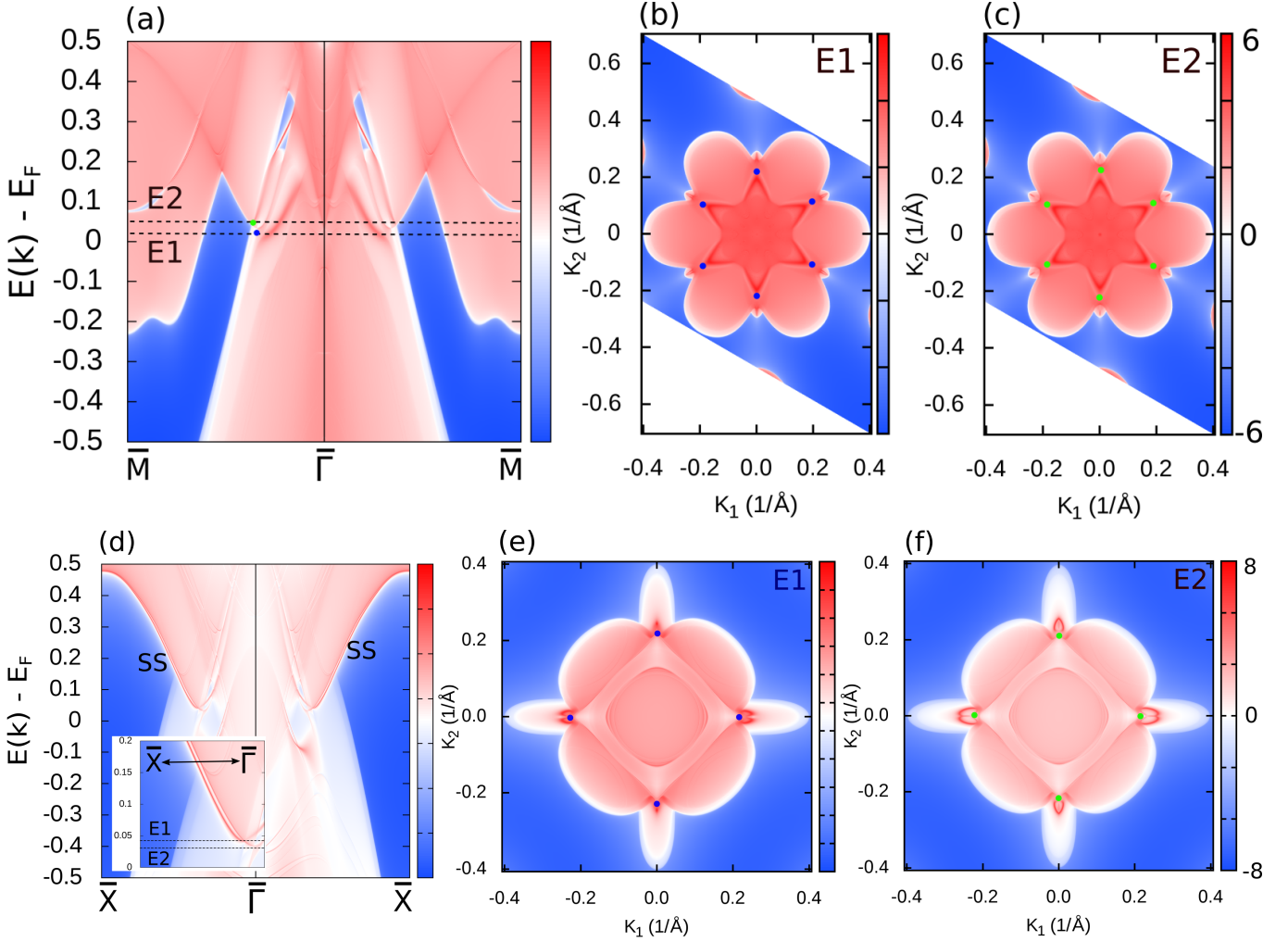


FIG. 3. (Color online) Surface density of states (a,d) and Fermi arcs (b,c and e,f) for (111) surface (top panel) and (001) surface (bottom panel). The constant energy map at E1(E2) is for TP1(TP2). The triple points are marked by blue and green dots for two TPs.

simplest form and are expected to be more interesting for experimental probing.

Similar to the WSM, TPSMs also hold the signature of bulk band degeneracies onto its surfaces. Hence surface dispersion and Fermi arcs of TPSM are worthy of careful investigation both from theoretical and experimental front. Since a TP is equivalent to superposition of two

degenerate Weyl points, a natural expectation is the appearance of two Fermi arc from a typical TP. These two Fermi arcs, originated from a TP, are further expected to connect with two other nearest TPs in the Surface BZ. In Fig. 3, we present the surface density of states and the Fermi arcs of (111) and (001) surface. Energy scales of TPs on surfaces are indicated by dashed reference lines (E1 & E2). For (111) surface in Fig. 3(a), a pair of surface state originates from two TPs and disperse along $\bar{\Gamma}$ point and they are supposed to be degenerate at the zone center as $\bar{\Gamma}$ is one of the time reversal point of the (111) surface BZ. But they get masked by the bulk bands and disappear near $\bar{\Gamma}$ as they propagate from zone boundary to zone center. However, the degeneracy of these two TP induced surface states are clear at \bar{X} in (001) surface spectrum as shown in Fig. 3(d). Here, a pair of surface state (SS) emerges from two TPs and disperse towards \bar{X} (as shown in inset of Fig. 3(d)) and become degenerate at \bar{X} as it is one of the four TRIM point of (001) sur-

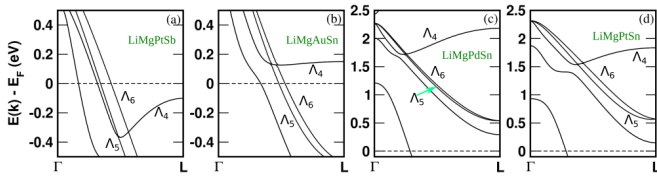


FIG. 4. (Color online) Bulk band structure of (a) LiMgPtSb, (b) LiMgAuSn, (c) LiMgPdSn and (d) LiMgPtSn with spin-orbit coupling. The pair of triple points are shown at the crossing of Λ_4 and $\Lambda_{5,6}$ IRs along Γ -L direction.

face BZ. Fig. 3(b,c) and 3(e,f) show the constant energy contour map at energy $E_1=0.033$ eV and $E_2=0.041$ eV corresponding to TP1 and TP2 respectively. As shown in Fig. 3(b-c), the Fermi arcs appear from each six TPs projected on (111) surface and they merged to the nearest TPs to form a hexagon shape surrounding the Γ point. The nature of Fermi arcs are further preserved by C_3 symmetry in (111) surface. However, for (001) surface four TPs are projected on surface BZ. The projection of TPs are also schematically shown in Fig. 1(b). These four projected TPs on (001) surface are connected by Fermi arcs which is different in shape compare to (111) surface Fermi arcs, as illustrated in Figure 3(e-f).

In addition to LiMgPdSb, we have investigated several other compounds in the quaternary Heusler class and found four of them quite interesting. These compounds indeed show similar TPs, but at much different momenta distance and both the +ve and -ve side of the E_F . These compounds are LiMgPtSb, LiMgAuSn, LiMgPdSn, and LiMgPtSn, whose SOC band structures are shown in Fig. 4. The optimized lattice parameter, and the location of TPs in terms of energy position ($\Delta\epsilon$) with respect to E_F and momenta distance Δ_k along Γ -L are shown in Table I. These TPs being away from the

Γ -point, should be easier to probe and hence awaits experimental confirmation.

Conclusion: In summary, we show the occurrence of triple point Fermionic state in quaternary Heusler alloys. The symmetry protected band degeneracies are the recipe of TP formation. We found, along Γ -L direction, two bands from two different IRs (Λ_4 and $\Lambda_{5,6}$) of C_{3v} point group crosses each others and hence form triple point. The surface states on (111) and (100) miller plane are investigated and shown. The projected TPs on (111) surface revealed a hexagonal shape Fermi arcs which is a band topology mediated phenomena arises due to the non-trivial band degeneracies. The shape of Fermi arcs depends on the type of cleaved surface and hence the number of TPs projected on the surface. The observed TPs in our system of interest are far away from the Brillouin zone center along C_3 axes. Thus, we believe that quaternary Heusler alloy provide an ideal platform for triple point Fermionic state and demands strong experimental investigation using photoemission spectroscopy and tunneling microscopy.

C.K.B and C.M acknowledge MHRD-India for financial support.

-
- * These two authors have contributed equally to this work
 \dagger aftab@iitb.ac.in
- ¹ M. Z. Hasan and C. L. Kane, Colloquium: Topological insulators, *Rev. Mod. Phys.* **82**, 3045 (2010).
 - ² X. Qi and S.-C. Zhang, Topological insulators and superconductors, *Rev. Mod. Phys.* **83**, 1057-1110 (2011).
 - ³ J. E. Moore, The birth of topological insulators, *Nature* **464**, 194-198 (2010).
 - ⁴ A. Bansil, Hsin Lin, and Tanmoy Das, Colloquium: Topological band theory, *Rev. Mod. Phys.* **88**, 021004 (2016).
 - ⁵ S. M. Young, S. Zaheer, J. C. Y. Teo *et.al.* *Phys. Rev. Lett.* **108**, 140405 (2012).
 - ⁶ Bohm-Jung Yang and Naoto Nagaosa, *Nat. Commun.* **5**, 4898 (2014).
 - ⁷ Z. K. Liu, B. Zhou, Y. Zhang *et.al.* *Science* **343** 864(2014).
 - ⁸ S. -Y. Xu, C. Liu, S. K. Kushwaha *et.al.* *Science* **347** 294(2015).
 - ⁹ Madhab Neupane, Su-Yang Xu, Raman Sankar *et.al.* *Nat. Commun.* **5**, 3786 (2014).
 - ¹⁰ Z. K. Liu, J. Jiang, B. Zhou *et.al.* *Nat. Materials* **13** 677 (2014).
 - ¹¹ Congcong Le, Shengshan Qin, Xianxin Wu *et.al.* *Phys. Rev. B* **96**, 115121 (2017).
 - ¹² K.-W. Chen, X. Lian, Y. Lai *et.al.* *Phys. Rev. Lett.* **120** 206401 (2018).
 - ¹³ N.P. Armitage, E.J. Mele, and Ashvin Vishwanath, *Rev. Mod. Phys.* **90**, 015001 (2018).
 - ¹⁴ Peng Li, Yan Wen, Xin He *et.al.* *Nat. Commun.* **8**, 2150 (2017).
 - ¹⁵ Alexey A. Soluyanov, Dominik Gresch, Zhijun Wang *et.al.* *Nature* **527**, 495 (2015).
 - ¹⁶ Su-Yang Xu, Ilya Belopolski, Nasser Alidoust *et.al.* *Science* **349**, 613 (2015).
 - ¹⁷ Xiangang Wan, Ari M. Turner, Ashvin Vishwanath, and Sergey Y. Savrasov, *Phys. Rev. B* **83**, 205101 (2011).
 - ¹⁸ B. Singh, A. Sharma, H. Lin *et.al.* *Phys. Rev. B* **86**, 115208 (2012).
 - ¹⁹ H. Weng, C. Fang, Z. Fang *et.al.* *Phys. Rev. X* **5**, 011029 (2015).
 - ²⁰ J. Liu and D. Vanderbilt, *Phys. Rev. B* **90**, 155316 (2014).
 - ²¹ Rui Yu, Hongming Weng, Zhong Fang *et.al.* *Phys. Rev. Lett.* **115**, 036807 (2015).
 - ²² Youngkuk Kim, Benjamin J. Wieder, C. L. Kane, and Andrew M. Rappe, *Phys. Rev. Lett.* **115**, 036806 (2015).
 - ²³ Guang Bian, Tay-Rong Chang, Hao Zheng *et.al.* *Phys. Rev. B* **93**, 121113(R) (2016).
 - ²⁴ Guang Bian, Tay-Rong Chang, Raman Sankar *et.al.* *Nat. Commun.* **7**, 10556 (2016).
 - ²⁵ Jian-Tao Wang, Hongming Weng, Simin Nie, Zhong Fang *et.al.* *Phys. Rev. Lett.* **116**, 195501 (2016).
 - ²⁶ Huaqing Huang, Kyung-Hwan Jin, and Feng Liu, *Phys. Rev. B* **96**, 115106 (2017).
 - ²⁷ Qiunan Xu, Rui Yu, Zhong Fang *et.al.* **95**, 045136 (2017).
 - ²⁸ Lin-Lin Wang, Adam Kaminski, Paul C. Canfield, and Dwayne D. Johnson, *J. Phys. Chem. C* **122** 705 (2018).
 - ²⁹ Ziming Zhu, Georg W. Winkler, QuanSheng Wu *et.al.* *Phys. Rev. X* **6**, 031003 (2016).
 - ³⁰ Guoqing Chang, Su-Yang Xu, Shin-Ming Huang *et.al.* *Sci. Rep.* **7**, 1688 (2017).
 - ³¹ Hongming Weng, Chen Fang, Zhong Fang, and Xi Dai, *Phys. Rev. B* **93**, 241202(R) (2016).
 - ³² Georg W. Winkler, QuanSheng Wu, Matthias Troyer *et.al.* *Phys. Rev. Lett.* **117**, 076403 (2016).
 - ³³ Xiaoming Zhang, Zhi-Ming Yu, Xian-Lei Sheng *et.al.* *Phys. Rev. B* **95**, 235116 (2017).
 - ³⁴ Yunyouyou Xia and Gang Li, *Phys. Rev. B* **96**, 241204(R)

- (2017).
- ³⁵ Jianfeng Wang, Xuelei Sui, Wujun Shi *et.al.* Phys. Rev. Lett. **119**, 256402 (2017).
- ³⁶ Peng-Jie Guo, Huan-Cheng Yang, Kai Liu, and Zhong-Yi Lu, Phys. Rev. B **98**, 045134 (2018).
- ³⁷ Hongming Weng, Chen Fang, Zhong Fang, and Xi Dai, Phys. Rev. B **94**, 165201 (2016).
- ³⁸ B. Q. Lv, Z.-L. Feng, Q.-N. Xu *et.al.* Nature Letter **546**, 627 (2017).
- ³⁹ Huaqing Huang, Kyung-Hwan Jin, and Feng Liu, Phys. Rev. Lett. **120**, 136403 (2018).
- ⁴⁰ QuanSheng Wu, Christophe Piveteau, Zhida Song, and Oleg V. Yazyev1, Phys. Rev. B **98**, 081115(R) (2018).
- ⁴¹ Saad Zaheer, S. M. Young, D. Cellucci *et.al.* Phys. Rev. B **87**, 045202 (2013).
- ⁴² Hao Yang, Jiabin Yu, Stuart S. P. Parkin *et.al.* Phys. Rev. Lett. **119**, 136401 (2017).
- ⁴³ Zhi-Gang Song, Claudia Felser, and Yan Sun, arXiv:1808.01163v1
- ⁴⁴ G. Kresse and J. Hafner, Phys. Rev. B **47**, 558(R) (1993)
- ⁴⁵ G. Kresse and D. Joubert, Phys. Rev. B **59**, 1758 (1999)
- ⁴⁶ P. E. Böchl, Phys. Rev. B **50**, 17953 (1994).
- ⁴⁷ Nicola Marzari and David Vanderbilt, Phys. Rev. B **56**,12847 (1997).
- ⁴⁸ Ivo Souza, Nicola Marzari, and David Vanderbilt, Phys. Rev. B **65**, 035109 (2001).
- ⁴⁹ Nicola Marzari, Arash A. Mostofi, Jonathan R. Yates, Ivo Souza, and David Vanderbilt, Rev. Mod. Phys. **84**, 1419 (2012).
- ⁵⁰ D. H. Lee and J. D. Joannopoulos, Phys. Rev. B **23**, 4988 (1981).
- ⁵¹ D. H. Lee and J. D. Joannopoulos, Phys. Rev. B **23**, 4997 (1981).
- ⁵² M P Lopez Sancho, J M Lopez Sancho, J M L Sancho and J Rubio, J. Phys. F:Met. Phys. **15**, 851 (1985).
- ⁵³ QuanSheng Wu, ShengNan Zhang, Hai-Feng Song, Matthias Troyer, Alexey A. Soluyanov, arXiv:1703.07789 2017.
- ⁵⁴ Tanja Graf, Claudia Felser, Stuart S.P. Parkin, Progress in Solid State Chemistry **39**, 1-50 (2011).